

Improving the Coastal Mean Dynamic Topography by Geodetic Combination of Tide Gauge and Satellite Altimetry

Ole B. Andersen, Karina Nielsen, Per Knudsen, Chris W. Hughes, P. L. Woodworth, Rory Bingham, Luciana Fenoglio-Marc, M d ric Gravelle, Michael Kern, and Sara Padilla Polo

QUERY SHEET

This page lists questions we have about your paper. The numbers displayed at left can be found in the text of the paper for reference. In addition, please review your paper as a whole for correctness.

- 1248
- 1249
- 1250
- 1251
- 1252
- 1253
- 1254
- 1255
- 1256
- 1257
- 1258
- 1259
- 1260
- 1261
- 1262
- 1263
- 1264
- 1265
- 1266
- 1267
- 1268
- 1269
- 1270
- 1271
- 1272
- 1273
- 1274
- 1275
- 1276
- 1277
- 1278
- 1279
- 1280
- 1281
- 1282
- 1283
- 1284
- 1285
- 1286
- 1287
- 1288
- 1289
- 1290
- Q1.** Please check whether article title has been OK as typeset as the title given in title page document ends with the word "estimates." Kindly check and amend if necessary.
- Q2.** Please note that there is a mismatch in number of authors between CATS and manuscript hence one in the manuscript has been retained. Kindly check whether the author names (first name followed by last name) and affiliations are correct as presented in the proofs. Kindly provide department name for all the affiliations.
- Q3.** Please check and resupply the corresponding author's email and postal address if the given is inaccurate.
- Q4.** Please check that the heading levels have been correctly formatted throughout.
- Q5.** Please provide the place of publication for Andersen et al. 2016.
- Q6.** Please provide the volume and page numbers for reference "Dinardo et al. 2017."
- Q7.** Please provide the volume and page numbers for reference "Fenoglio-Marc and Buchhaupt 2017."
- Q8.** Please update reference "Filmer et al. 2018," if possible.
- Q9.** Please provide the volume or page numbers as appropriate for "Foerste 2014."
- Q10.** Please provide publisher name and location in reference "IERS 2010."
- Q11.** Please provide volume number in reference "Woodworth et al. 2017."

1291
1292
1293
1294
1295
1296
1297
1298
1299
1300
1301
1302
1303
1304
1305
1306
1307
1308
1309
1310
1311
1312
1313
1314
1315
1316
1317
1318
1319
1320
1321
1322
1323
1324
1325
1326
1327
1328
1329
1330
1331
1332
1333

TABLE OF CONTENTS LISTING

The table of contents for the journal will list your paper exactly as it appears below:

Improving the Coastal Mean Dynamic Topography by Geodetic Combination of Tide Gauge and Satellite Altimetry

Ole B. Andersen, Karina Nielsen, Per Knudsen, Chris W. Hughes, P. L. Woodworth, Rory Bingham, Luciana Fenoglio-Marc, Médéric Gravelle, Michael Kern, and Sara Padilla Polo



Improving the Coastal Mean Dynamic Topography by Geodetic Combination of Tide Gauge and Satellite Altimetry

Q1

Ole B. Andersen^a, Karina Nielsen^a, Per Knudsen^a, Chris W. Hughes^{b,c}, P. L. Woodworth^c, Rory Bingham^d, Luciana Fenoglio-Marc^e, Médéric Gravelle^f, Michael Kern^g, and Sara Padilla Polo^h

Q2

^aTechnical University of Denmark, DTU Space, Lyngby, Denmark; ^bUniversity of Liverpool, Liverpool, UK; ^cNational Oceanography Centre, Liverpool, UK; ^dUniversity of Bristol, Bristol, UK; ^eUniversity of Bonn, Bonn, Germany; ^fLIENSs, Université de La Rochelle-CNRS, La Rochelle, France; ^gESA ESTEC, Noordwijk, The Netherlands; ^hLEGOS, CNRS-CNES-IRD-UPS, Toulouse, France

ABSTRACT

The ocean mean dynamic topography (MDT) is the surface representation of the ocean circulation. The MDT may be determined by the ocean approach, which involves temporal averaging of numerical ocean circulation model information, or by the geodetic approach, wherein the MDT is derived using the ellipsoidal height of the mean sea surface (MSS), or mean sea level (MSL) minus the geoid as the geoid. The ellipsoidal height of the MSS might be estimated either by satellite or coastal tide gauges by connecting the tide gauge datum to the Earth-centred reference frame. In this article we present a novel approach to improve the coastal MDT, where the solution is based on both satellite altimetry and tide gauge data using new set of 302 tide gauges with ellipsoidal heights through the SONEL network. The approach was evaluated for the Northeast Atlantic coast where a dense network of GNSS-surveyed tide gauges is available. The typical misfit between tide gauge and satellite or oceanographic MDT was found to be around 9 cm. This misfit was found to be mainly due to small scale geoid errors. Similarly, we found, that a single tide gauge places only weak constraints on the coastal dynamic topography.

ARTICLE HISTORY

Received 26 March 2018
Accepted 26 September 2018

KEYWORDS

Mean dynamic topography;
satellite altimetry;
tide gauge

Q4 Introduction

The ocean's mean dynamic topography (MDT) is the surface representation of ocean circulation. It is of interest to oceanographers to study the ocean's surface currents (Wunsch and Stammer 1997), and to geodesists for example linking height datums globally, particularly in regions where geodetic land-ties (connection by levelling to the land vertical datum) through

CONTACT Ole B. Andersen  oa@space.dtu.dk  DTU Denmark, Elektrovej Building 328, DK-2800 Kongens Lyngby, Denmark.

Q3

Color versions of one or more of the figures in the article can be found online at www.tandfonline.com/umgd.

© 2018 Taylor & Francis Group, LLC

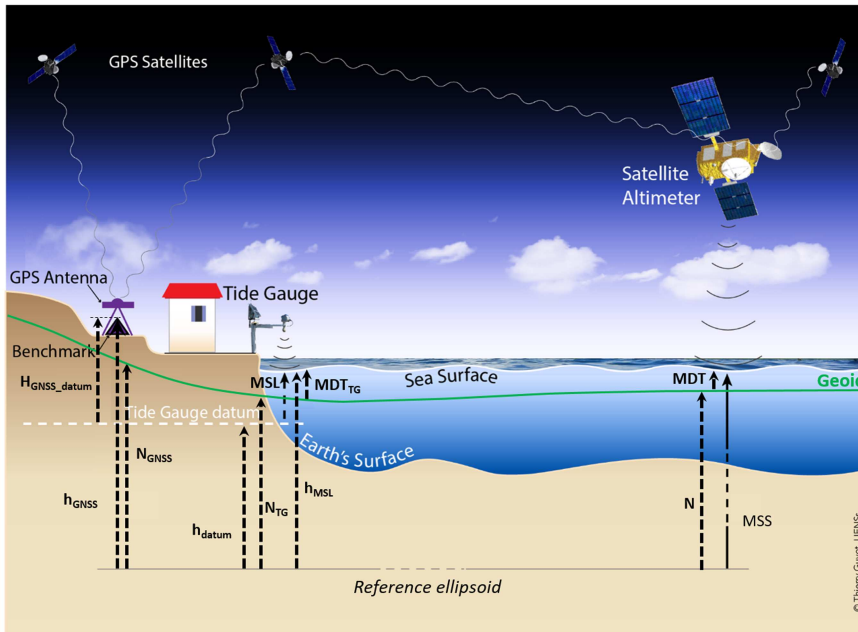


Figure 1. Satellite and tide gauge observations of the ellipsoidal mean sea surface (MSS) or mean sea level (MSL) relative to the tide gauge datum. The geoid height is called (N); the figure shows the terms of the equations derived in Tide Gauge MDT section. The figure is modified from Thierry Guyot (LIENSs).

GNSS measured tide gauges are not possible (Featherstone and Filmer 2012; Woodworth et al. 2013).

The ocean MDT may be determined by the oceanographic approach or the geodetic approach (Huang 2017; Woodworth et al. 2013). The oceanographic approach involves the use of an ocean circulation models and the MDT is computed through temporal averaging over a given period.

The geodetic approach involves either satellite derived ellipsoidal mean sea surface models (MSS) (Andersen and Knudsen 2009) or mean sea level (MSL) observations from tide gauges expressed as ellipsoidal heights from colocated GNSS observations.

Figure 1 illustrates the way that the MSS or MSL is determined using geodetic methods like satellite altimetry and tide gauges. Once referenced to the same reference ellipsoid MSS and MSL represent the same “quantity,” but in the following we have used the terminology MSL for individual point observations (from tide gauges) and MSS for satellite derived grids.

From the ellipsoidal MSS or MSL data the MDT can be derived through a purely geometrical approach based on the simple equation

$$\text{MDT} = \text{MSS} - N \quad (1)$$

87 The MSS and/or MSL and geoid (N) must be given relative to same tide
88 system and with respect to the same reference ellipsoid. We used the mean
89 tide system and the TOPEX ellipsoid, with a semi major axis of
90 6,378,136.3 m and an inverse flattening of 298.257. Other ellipsoids or tide
91 systems can be used through transformation. GNSS measurements, that are
92 initially consistent with the WGS84 reference frame, are usually aligned
93 with the International Terrestrial Reference Frame (ITRF) for Earth science
94 applications that require a high degree of accuracy (IERS 2010). Thus, the
95 GNSS ellipsoidal heights were here transformed to the most up-to-date
96 ITRF realisation at the time of the study (the ITRF08 (Altamimi, Collilieux,
97 and Métivier 2011), which is associated with the GRS80 ellipsoid). In
98 comparison or integration with satellite derived MDT these height are then
99 converted to be consistent with the TOPEX ellipsoid and the mean-tide
100 system following (Ekman 1989).

101 This work continues the attempt to improve the coastal mean dynamic
102 topography supporting ESA effort in the use of geoid information for height
103 system unifications and connections (Amjadiparvar et al. 2013; Gerlach and
104 Rummel 2013; Gruber, Gerlach, and Haagmans 2012; Rummel 2012). New
105 and more accurate geoid information is applied from the ESA mission
106 Gravity field and Ocean Circulation Explorer (GOCE) made available via the
107 international centre for global Earth Models (IGCEM, [http://icgem.gfz-
108 potsdam.de/home](http://icgem.gfz-potsdam.de/home)). We test a novel approach to derive an improved coastal
109 MDT along the Northeast European coast using a geodetic combination
110 of a satellite MDT at sea combined with a number of tide gauges derived
111 MDT values along the coast. In the following, we refer to this combined
112 geodetic approach as the GOCE++ approach as the work describes the
113 result of the GOCE++ study initiated by the European Space Agency (ESA).

114 We chose a common 5-year period 2003–2007 inclusive for this investiga-
115 tion for consistency. The period was chosen as it offered the highest number
116 of near-uninterrupted tide gauges with ellipsoidal height from GNSS. Out
117 MDT will consequently represent this period. higher Initially, data and meth-
118 ods are described along with the way the MDT is determined geodetically
119 from satellite and from tide gauges. For the chosen time period we then pre-
120 sent the updated set of 302 tide gauges with known ellipsoidal heights from
121 the GNSS data assembly centre for the Global Sea Level Observing System at
122 the Système d’Observation du Niveau des Eaux Littorales (SONEL, [http://
123 www.sonel.org](http://www.sonel.org)). Here we evaluate the degree to which the point measure-
124 ments of MDT at tide gauges can be reconciled with the broader scale
125 MDTs of ocean models and those derived from altimetry.

126 Subsequently we present an attempt to merge satellite MDT and tide
127 gauge MDT using an iterative method called GOCE++. The northeast
128 European shelf has a huge number of tide gauges including 100 ellipsoidal
129

130 tide gauges in the SONEL network. This enables us to perform a compari-
131 son of the effect on including tide gauges in the coastal MDT solution.

132 Currently, synthetic aperture radar (SAR) altimetry is becoming available
133 with Cryosat-2 and Sentinel-3 to improve the mapping of the short scales
134 in the MSS. These data are an important step to improve future coastal
135 MDT models and we present an evaluation of the MDT and improvements
136 in the southern North Sea.

137 138 **Data and methods**

139 In the following subsections, we introduce the various datasets and
140 methods to derive the MDT. We introduce the oceanographic MDT used
141 for comparison as well as the satellite tide gauge data and the way geodetic
142 MDT is computed.
143

144 145 ***Ocean MDT***

146 Seven ocean models were available for computation of MDT in the study.
147 These are three Nemo (Nucleus for European Modelling of the Ocean)
148 ORCA (Madec 2008) model integrations, one at a resolution of $1/4^\circ$
149 (NemoQ), and two at a resolution of $1/12^\circ$ with slightly different versions of
150 the model code (Nemo12a, Nemo12b). Two Liverpool University implemen-
151 tations of the Massachusetts Institute of Technology (MIT) global ocean
152 circulation model (Marshall et al. 1997a, 1997b), assimilating hydrographic
153 information provided by the UK Met Office (Smith and Murphy 2007); one
154 in a coarse form (LivC), with a global resolution of 1° and a finer version
155 (LivS) with an increased resolution of $1/5^\circ \times 1/6^\circ$ in the North Atlantic. The
156 final two models are products of the ECCO consortium to calculate ocean
157 state estimates by assimilating a wide variety of data, including geodetic data.
158 EccoG (ECCO-Godae) has a global resolution of 1° (Köhl, Stammer, and
159 Cornuelle 2007) producing a model state and evolution which is perfectly
160 consistent with the model equations. Ecco2 (Menemenlis, Fukumori, and Lee
161 2005a; Menemenlis et al. 2005b) is a finer resolution model (specified
162 as ~ 18 km, but supplied on a 0.25 degree grid), with a looser assimilation
163 scheme designed to match only certain patterns within the observations.
164 All ocean models incorporate climatology for their initiation, as well as wind
165 and atmospheric forcing from meteorological reanalyses. All models are
166 averaged over the chosen period of 2003–2007 inclusive.
167

168 169 ***Satellite MDT***

170 Computing the satellite MDT is conceptually simple with the use of
171 Eq. (1). However, there are several complications in computing the satellite
172

MDT. The major complication is the fact, that the geoid is typically given with limited resolution (typically hundreds of kilometers) compared to the MSS (tens of kilometers).

Subtracting a geoid N given in spherical harmonic coefficients up to a certain degree and order L the resulting dynamic topography estimate,

$$\text{MDT}_R = \text{MDT} + \Delta\text{NL}, \quad (2)$$

where the derived MDT_R consists of the MDT plus an un-modelled part of the geoid of spherical harmonic degrees and orders higher than L appearing as an omission error due to spherical harmonic coefficients which are omitted in the geoid model. This error decreases with increasing degree and order L of the geoid. The GOCE satellite has been paramount to reduce the geoid error in global geoids where the degree and order of satellite only GOCE geoids is typically around 250.

Consequently, a filter needs to be derived and applied to Eq. (2) to eliminate the ΔNL without removing real MDT signal in the filtering. It is naturally important to design appropriate linear or non-linear filters for this operation (Bingham and Haines 2006; Bingham et al. 2011; Sanchez-Reales, Andersen, and Vigo 2016).

We decided to use the alternative approach to limit the omission error ΔNL by using a geoid and a MSS given at the same resolution. We used the European Improved Gravity model of the Earth by New techniques (EIGEN) combined 6C4 geoid to degree and order 2190 due to consistency with the MSS. This EIGEN6C4 geoid (Foerste 2014) consists of a combination of GRACE and GOCE up to degree and order 260 augmented with the DTU10 surface gravity data. For the investigation, we used the DTU10MSS (Andersen and Knudsen 2009; Andersen, Knudsen, and Stenseng 2016). This is computed as an average of satellite altimetry over the period 1993–2009; but is mapped to the 2003–2007 average by using the difference in AVISO (Archiving, Validation, and Interpretation of Satellite Oceanographic data) absolute dynamic topography (ADT) averages over the two periods. DTU10MSS was preferred because this model is consistent with various geoids like the EIGEN6C4 and the TUM13 (Fecher, Pail, and Gruber 2015) geoid (the gravity anomaly dataset is derived from the DTU10MSS, so the difference does not add artificial small-scale errors into the dynamic topography).

Altimetric MSS is corrected for the ocean's inverted barometer (IB) response (static atmospheric loading effect) using Wunsch and Stammer (1997) and a correction for periods shorter than the sampling of the Topex and Jason satellite via the Dynamic Atmosphere Correction. This correction is applied, as it reduces the sea surface variability leading to a more stable estimation of the mean. In our approach, we decided to restore the effect of the atmosphere on the sea surface to be consistent with the tide gauge mean.

216 The total error of the satellite derived MDT will be a combination of the
217 geoid omission errors along with errors in both the MSS and the geoid
218 coefficients (commission errors). The satellite MDT is typically less accurate
219 in the coastal zone due to a combination of less accurate altimetric observa-
220 tions, less accurate geoid mapping due to large bathymetry/topography varia-
221 tions and the fact that the MDT changes more rapidly in the coastal zone.
222

223 ***Tide gauge MDT***

224 Using global tide gauges for comparisons and combination with satellite
225 MDT implies that the tide gauges height is linked into a Earth-centred
226 global reference frame using GNSS measurements at the local tide gauges
227 transforming the observations to ellipsoidal heights. This link usually relies
228 on two quantities: the GNSS-derived ellipsoidal height of a tide gauge
229 benchmark in the global reference (h_{GNSS} in Figure 1), obtained from the
230 processing of permanent or episodic GNSS measurements, and the height
231 of this benchmark with respect to the tide gauge datum ($H_{\text{GNSS_datum}}$ in
232 Figure 1). The latter is always known from the Permanent Service for
233 Mean Sea Level (PSMSL) (Holgate et al. 2013) When the benchmark height
234 is not available, a supplemental measurement is needed to connect this
235 benchmark to one where GNSS ellipsoidal height is known (mostly using
236 spirit levelling). This is commonly called a geodetic tie (Woodworth et al.
237 2017), and ultimately yields A in Figure 1.
238
239

240 ***Tide gauges with permanent GNSS***

241 The use of GNSS for monitoring the tide gauge sites stability is optimised
242 when it is processed continuously and globally (Wöppelmann and Marcos
243 2016). Thus, the availability of positions and vertical velocity of tide gauge
244 co-located permanent GNSS stations was a priority for the investigation.
245 The geodetic ties of 113 RLR tide gauges with nearby permanent GNSS
246 stations were collected from the SONEL data assembly centre (<http://www.sonel.org>).
247 Fourteen additional ties were recovered for the German tide
248 gauges, which are not in the RLR dataset yet (<http://pegelonline.wsv.de>).
249 For most of these permanent GNSS stations, the ellipsoidal height
250 (associated to an epoch and an uncertainty) was extracted from the last
251 GPS solution (ULR6a) of the ULR analysis centre provided on SONEL
252 (Santamaría-Gómez et al. 2017). The vertical velocities were then used to
253 propagate the ellipsoidal height from the reference epoch to the average
254 epoch of the selected period 2003–2007 (2005.5). For permanent stations,
255 that were not included in this solution, the ellipsoidal heights were
256 obtained from the average of three positions per day, processed using the
257 Canadian CSRS-PPP tool (<https://webapp.geod.nrcan.gc.ca/geod/tools->
258

259 outils/ppp.php), also expressed in the ITRF08 reference frame. For the
 260 ULR6 stations that did not satisfy the “robust” velocity criteria defined by
 261 SONEL, the propagation to the epoch 2005.5 could not be performed and
 262 the stations were rejected.

264 *Tide gauges with episodic measurements*

265 Ellipsoidal heights from GNSS campaigns at tide gauge sites were retrieved
 266 from different sources; mostly via Woodworth et al. (2013, 2015),
 267 Featherstone and Filmer (2012), Lin et al. (2015) and SONEL, and led to
 268 189 additional RLR ellipsoidal heights.

269 For most of the ellipsoidal heights coming from episodic GNSS measure-
 270 ments, the epoch and the uncertainty is unknown. This is a source of error,
 271 and it was not possible to propagate the heights to the mean epochs of the
 272 selected period (they were adopted as is, as for permanent GNSS stations
 273 without enough data to obtain a robust velocity and the heights coming
 274 from the CSRS-PPP tool). These stations were associated with a cm uncer-
 275 tainty (arbitrary based on our personal experience).

278 *Computing the mean sea level*

279 For the RLR stations, the monthly time series from PSMSL were used to
 280 compute the MSL over the 2003–2007 period. For records with more than
 281 70% of data over this period, a classic average was calculated. For the remain-
 282 der 54 stations we applied simultaneous observations from satellite altimetry
 283 data to fill the gap. This was done in three stages: first, a least squares fit of
 284 IB-corrected tide gauge data on an annual cycle, semiannual cycle, linear
 285 trend, and altimeter time series was computed for every altimeter point
 286 (using the AVISO gridded dynamic topography, www.aviso.altimetry.fr/en)
 287 within 150 km of the tide gauge. Second, the altimeter point for which the
 288 resulting fit explained the largest percentage variance of the tide gauge data
 289 was selected, and tide gauge data predicted from that least squares fit for
 290 every month. Third, the predicted tide gauge time series was used to fill gaps
 291 in the tide gauge data, with an additional linear trend added over each gap to
 292 ensure the bestfit the end points. This yield a dataset of 302 ellipsoidal MSL
 293 values for the 2003–2007 period globally distributed (Figure 2).

295 Following Eq. (1), the MDT computation at a tide gauge implies sub-
 296 tracting the geoid height from the ellipsoidal MSL. Thus, at a tide gauge
 297 site, Eq. (1) can be written as follows (Figure 1):

$$298 \text{MDT}_{\text{TG}} = h_{\text{MSL}} - N_{\text{TG}} \quad (3)$$

299 where MDT_{TG} is the MDT value at the tide gauge, h_{MSL} is the tide gauge
 300 ellipsoidal MSL and N_{TG} is the geoid value at the tide gauge. h_{MSL} can be
 301

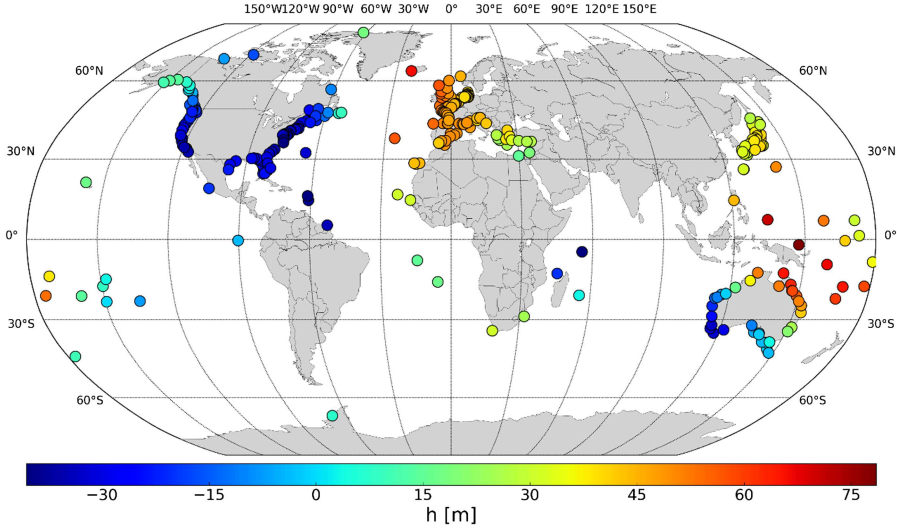


Figure 2. Ellipsoidal Mean sea level at tide gauges over (2003–2007).

developed as follows:

$$h_{\text{MSL}} = h_{\text{datum}} + \text{MSL} \quad (4)$$

where h_{datum} is the ellipsoidal height of the datum of the tide gauge measurements and MSL value as observed by the tide gauge with respect to this datum.

h_{datum} is obtained by adding the ellipsoidal height of the nearby GNSS station (h_{GNSS}) and the ellipsoidal height difference between the points ($DH_{\text{dat-gnss}}$):

$$h_{\text{datum}} = h_{\text{GNSS}} + DH_{\text{dat-gnss}} \quad (5)$$

$DH_{\text{dat-gnss}}$ is equal to the geodetic tie used ($\text{tie}_{\text{dat-gnss}}$) only if it comes from differential GNSS (and the tie is geometric and expresses indeed a difference of ellipsoidal heights). If the geodetic tie comes from spirit levelling, it expresses a difference in elevations and the geoid gradient has to be taken into account:

$$DH_{\text{dat-gnss}} = \text{tie}_{\text{dat-gnss}} + N_{\text{TG}} - N_{\text{GNSS}} \quad (6)$$

where $\text{tie}_{\text{dat-gnss}}$ is the geodetic tie used. Here it comes from spirit levelling and N_{GNSS} is the geoid value at the tide gauge-co-located GNSS point from which the tie has been derived. At the end, Eq. (3) becomes:

$$\text{MDT}_{\text{TG}} = h_{\text{GNSS}} + \text{tie}_{\text{dat-gnss}} + \text{MSL} - N_{\text{TG}} \quad (7)$$

if the $\text{tie}_{\text{dat-gnss}}$ is a difference of ellipsoidal heights, and:

$$\text{MDT}_{\text{TG}} = h_{\text{GNSS}} + \text{tie}_{\text{dat-gnss}} + \text{MSL} - N_{\text{GNSS}} \quad (8)$$

345 if $\text{tie}_{\text{dat-gnss}}$ is a difference of elevations. Note that Eqs. (7) and (8) are the
346 same if the GNSS point is very close (few meters) to the tide gauge (in that
347 case, the geoid heights at the tide gauge (N_{TG}) and at the GNSS (N_{GNSS})
348 are equal).

349 Computing the MDT values at the tide gauges from the ellipsoidal MSL
350 implies identifying the type of the geodetic tie in order to determine
351 whether the geoid value has to be extracted at the tide gauge position or at
352 the colocated GNSS point. We assumed that the GNSS point was situated
353 in the vicinity of the tide gauge for episodic GNSS point and that the geoid
354 difference between the locations is negligible.

355 For some countries the tide gauges benchmark (if available) are not
356 linked to the national vertical datum. For such this suggested unification is
357 particularly important to establish a height system and enables such links.

358 For tide gauges with permanent GNSS stations, the geodetic ties were
359 explicitly accounted for, but for episodic GNSS it was assumed (for lack of
360 any other information) that no tie was necessary. In strong geoid gradients
361 areas, the impact could reach more than ten centimetres (Figure 13). The
362 importance of the geoid extraction point indicates the equal importance of
363 the correct position of the tide gauge: particular care has been taken to
364 check the coordinates of the 302 selected tide gauges.
365
366

367 **Evaluation and representativeness of tide gauge MDT**

368 The tide gauge measurements with geocentric position information dis-
369 cussed above have been converted to MDT estimates by subtracting a geoid
370 from the MSS thus defined, that is by applying Eqs. (7) or (8) as appropri-
371 ate. Here we evaluate the degree to which the point measurements of MDT
372 at tide gauges can be reconciled with the broader scale MDTs of ocean
373 models and those derived from altimetry, considering the effect of different
374 geoids and different truncations. Note that, for this comparison with mod-
375 els (most of which do not include atmospheric pressure as a forcing), we
376 again apply the IB correction to all MDTs derived from tide gauges
377 or altimetry.
378

379 As the global mean value of MDT from ocean models is ill-defined, we
380 subtract this off from all mapped products. To do this in a consistent way
381 given the different spatial domains of the different products, we first choose
382 a reference model with global coverage (Ecco2) and subtract off the global
383 mean MDT from this model. For other mapped products, we subtract off
384 the spatial average of the difference from the de-measured Ecco2, over their
385 common domain. For comparisons purely at tide gauge positions below,
386 we further subtract the median of differences from the tide gauge MDT
387

388 across all available sites, so statistics relate to the spatial variations in MDT
389 and not the absolute values.

390 In addition to the Aviso MDT, we also use a second altimeter-derived
391 MDT labelled here TUM13, which is formed from the DTU2010 MSS
392 minus the TUM13 geoid. This was smoothed with a spatially varying
393 Wiener filter chosen using a signal size estimate from the Nemo12a ocean
394 model and noise based on the assumption that variations in a known
395 smooth region of the Pacific are all noise. The same product was also used
396 in Filmer et al. (2018).

397 The ordering of the tide gauges follows the PSMSL coastal ordering. This
398 starts with Norway, running anticlockwise around Europe, Africa and Asia,
399 then covers Australia and the Pacific, before running anticlockwise around
400 the Americas starting with Alaska and ending with Arctic Canada, before
401 finally moving to Antarctica (the last point only). See Appendix 1 for
402 more detail.

403 Several considerations can be made immediately from Figure 3. The
404 match is generally good, but the tide gauges show a systematic high bias
405 between about numbers 182 and 200, corresponding to the Pacific Islands.
406 The two prominent downward spikes (121 and 138) are Aburatsubo (near
407 Tokyo) and Mikuni (fairly nearby, but on the opposite, north coast of
408 mainland Japan). Tectonic activity is an obvious concern, but the many
409 other Japanese records look good. Other “spikes” are common to tide
410 gauges and models, and represent excursions off the main coastline
411 to islands.

412 Table 1 shows summary statistics based on these comparisons. The dis-
413 tribution is clearly non-Gaussian, with long tails and a more compact cen-
414 tral region, leading to a high excess kurtosis (kurtosis-3; a Gaussian
415 distribution has an excess kurtosis of zero, [https://www.itl.nist.gov/div898/
416 handbook/eda/section3/eda35b.htm](https://www.itl.nist.gov/div898/handbook/eda/section3/eda35b.htm)). We see that the global MDTs which
417 produce the worst comparisons tend to have lower kurtosis, becoming
418 closer to Gaussian values. This provokes a tentative interpretation, that the
419 global MDT errors tend to be more Gaussian, and the errors at tide gauges
420 include more extreme values, probably due to missing fine-scale geoid
421 information. This will be investigated in more detail below.

422 It is clear, that the data are able to discriminate between models, espe-
423 cially when ignoring the tails of the distributions. By far the most import-
424 ant factor is the quality of the geoid, and in particular its fine scale
425 structure corresponding to limiting the omission error in Eq. (2). This is
426 similar to what was seen by Huang (2017). This is illustrated by Figure 4,
427 which repeats Figure 3 but with the EIGEN6-C4 geoid truncated at degree
428 300 roughly corresponding to the degree and order of a satellite only geoid
429 from GOCE.
430

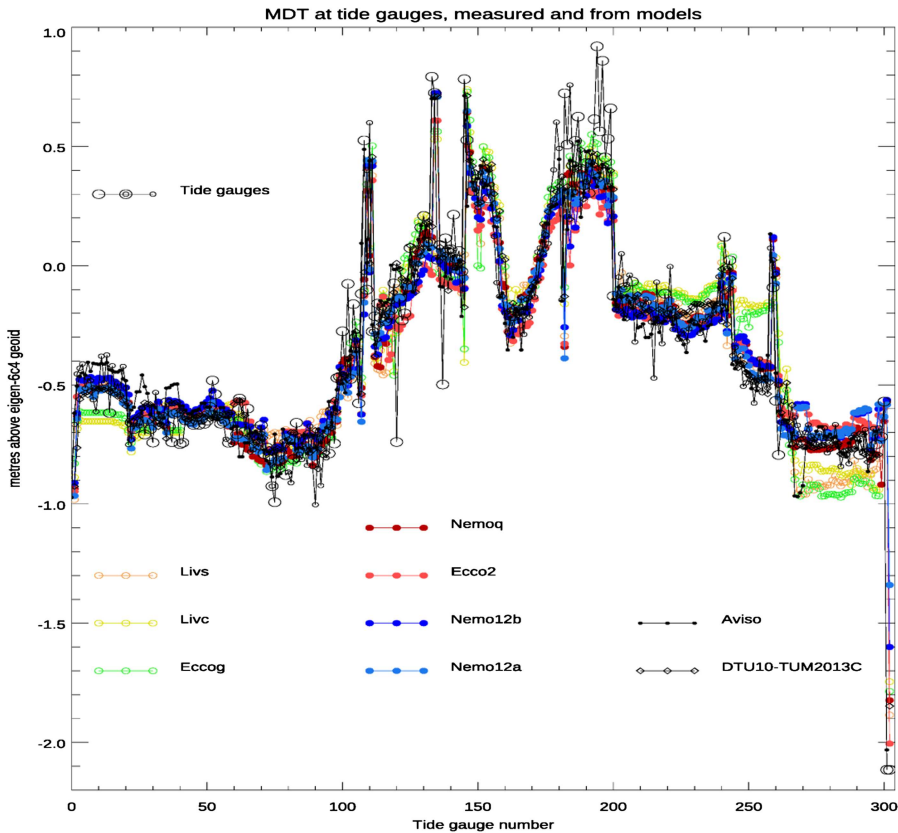
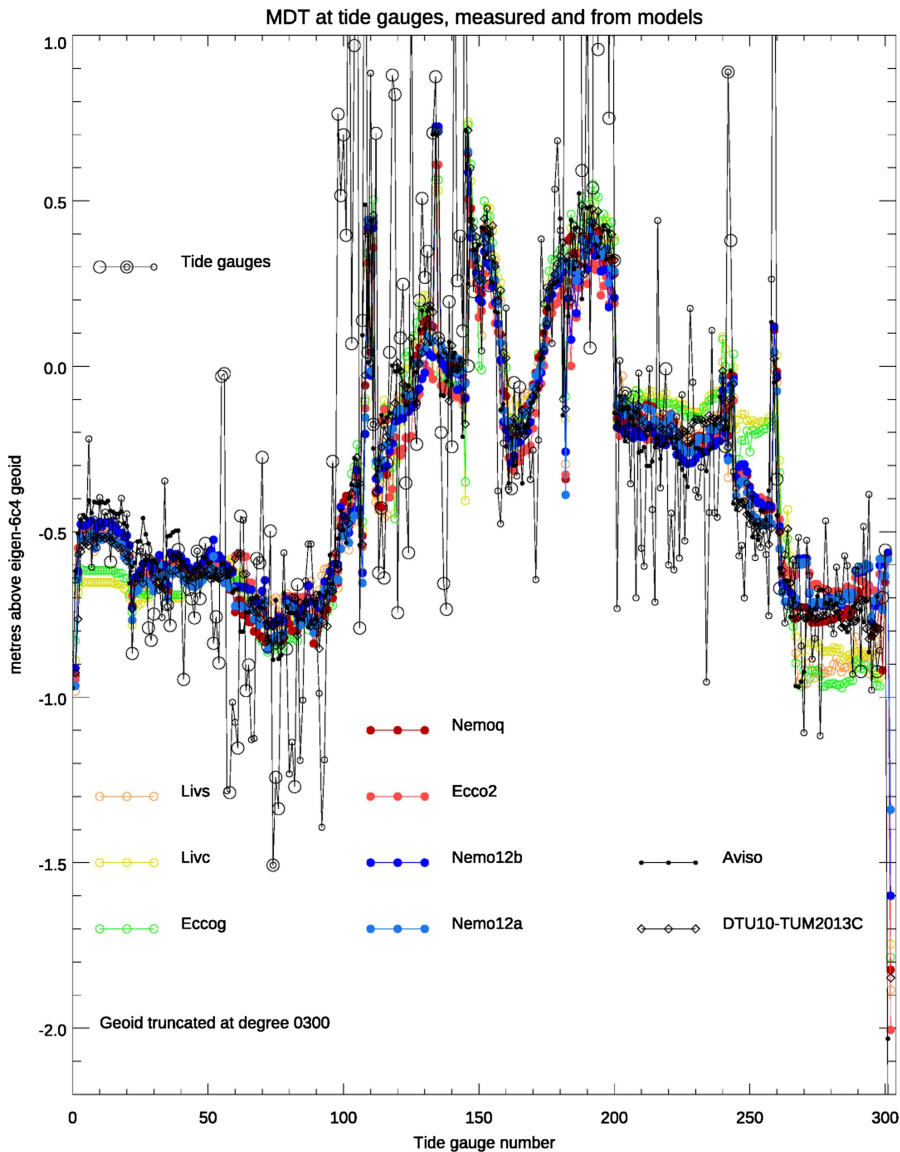


Figure 3. The MDT at 302 tide gauges (black open circles) using the EIGEN-6C4 geoid to its full resolution, compared with predictions from seven ocean models (colours), and two satellite-derived MDTs (black). Large open circles represent sites with continuous GNSS, and small open circles those with episodic GNSS. Continuous GNSS, but an estimated MSL/MSS error of >0.04 m is shown as a double circle (five sites).

Table 1. Statistics comparing the coastal MDT at tide gauges estimated using the EIGEN-6C4 geoid to full resolution, against 8 different global MDTs extrapolated to the same positions

Global MDT	Std	1 sigma	2 sigma	Min	Max	Skewness	Excess Kurtosis	N missing	% err <9 cm
Nemo12a	0.132	0.097	0.142	-0.775	0.571	-0.33	7.69	0	67
NemoQ	0.123	0.095	0.127	-0.588	0.617	+0.43	5.41	0	68
Aviso	0.134	0.099	0.131	-0.727	0.556	-0.21	6.27	3	65
DTU10TUM13	0.131	0.109	0.139	-0.726	0.589	+0.10	4.47	4	62
Nemo12b	0.139	0.101	0.157	-0.586	0.633	+0.60	4.45	0	64
Ecco2	0.145	0.121	0.153	-0.471	0.706	+0.99	3.18	1	54
Livs	0.161	0.132	0.177	-0.632	0.753	+0.75	3.24	3	54
EccoG	0.158	0.150	0.159	-0.600	0.540	-0.14	0.63	7	40
Livc	0.163	0.153	0.169	-0.572	0.546	-0.05	0.62	7	42

Height values are in metres. The pdfs are non-Gaussian, so they are characterised by half the range which contains the number of values which would be expected to fall within 1 sigma in a Gaussian distribution (one sigma equiv), or quarter the range for two sigma. Also given are the minimum and maximum values (TG-MDT after subtracting the median), and the number of missing values (because some MDTs do not have data in some regions). Where there are no missing values, there are 302 points being compared.



505 **Figure 4.** Repeat of Figure 3 but with the EIGEN-6c4 geoid truncated at degree 300.

506
507
508
509
510
511
512
513
514

The spatial distribution of the various MDT measurements can be seen from Figure 5. The map cannot show all details; however the general patterns are visible. We note that the MDT at the gauge on the east coast of South Africa (Richards Bay) agrees well with the Aviso global MDT, however the resolution of the thin strip of ocean to the west of the Agulhas current is crucial, as nearby ocean values are very different. More detailed examinations reveal similar results for the Gulf Stream, Kuroshio, and East Australian Current.

515
516

The distribution of misfits for these tide gauge values relative to the various global oceanographic MDT models is shown in Figure 6. A broader,

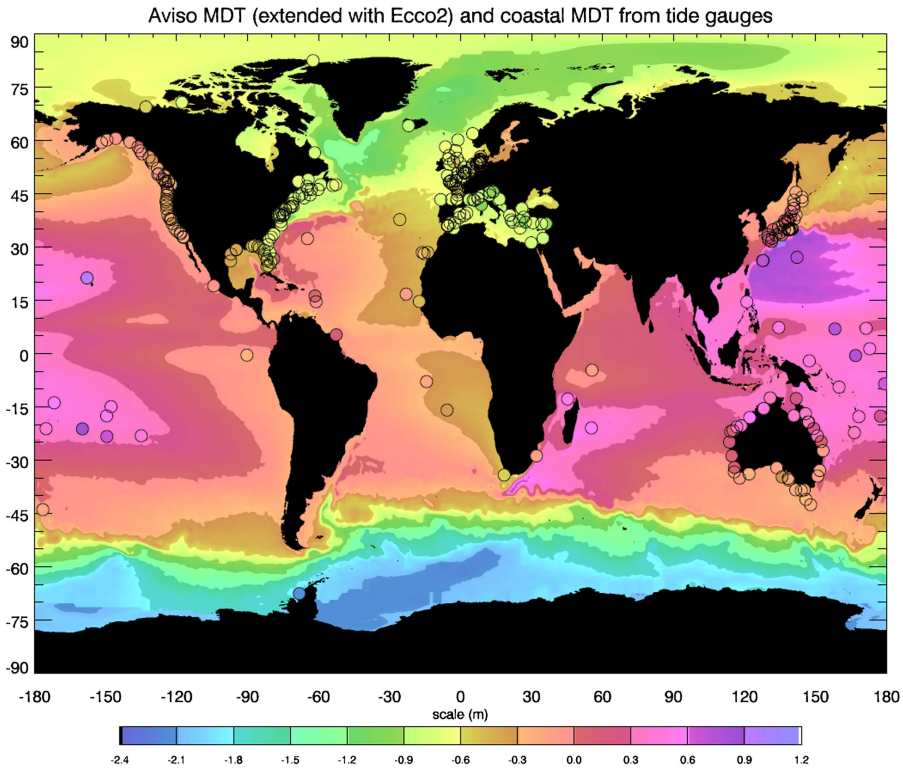


Figure 5. The spatial pattern of the Aviso MDT compared with the tide gauge MDT based on the EIGEN-6c4 geoid. Where the Aviso MDT has no data (mainly ice-covered regions), the Ecco2 model is shown instead.

more Gaussian distribution (peaks close to 1 with this normalization) are found with the coarse resolution models (livc, livs, eccog). It also illustrates the fact that the better comparisons (narrower distributions) have higher peaks than would be expected for a Gaussian distribution, consistent with the high kurtosis discussed above.

The PDFs in Figure 6 appear to have a longer positive tail than the associated negative tail. A long positive tail suggests that tide gauges are at positions, which are special in some way, leading to a systematic sign in the misfits, where they are large. We hypothesise that this is reflecting the fact that, being coastal, many tide gauges are close to the top of a steep continental slope, which produces a local geoid maximum at small length scales. In the absence of sufficient in situ gravity data, such maxima are likely to be reduced by smoothing, leading to the geoid product estimate being lower than the true geoid, and hence the MDT being higher than the true value.

With this interpretation, high kurtosis and a longer positive tail in the PDF would be diagnostic of an artificially smooth geoid. We can test this interpretation by calculating the statistics using various degrees of smoothing, produced by truncating the geoid at different resolutions. At the same

560
 561
 562
 563
 564
 565
 566
 567
 568
 569
 570
 571
 572
 573
 574
 575
 576
 577
 578
 579
 580
 581
 582
 583
 584
 585
 586
 587
 588
 589
 590
 591
 592
 593
 594
 595
 596
 597
 598
 599
 600
 601
 602

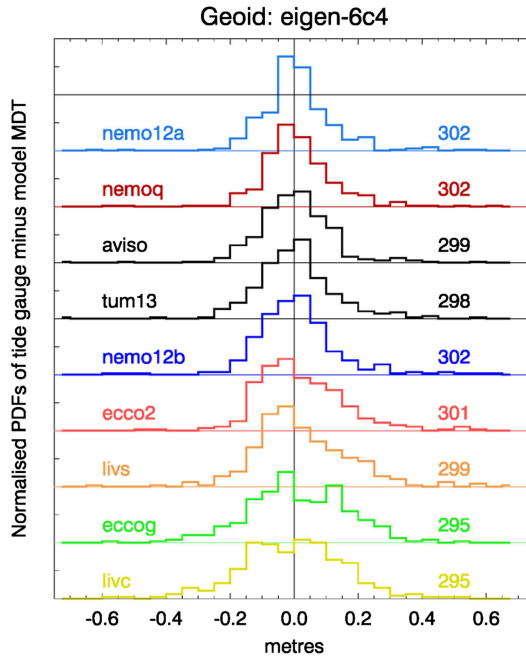


Figure 6. PDFs of the misfits between the tide gauge MDT using the EIGEN-6C4 geoid to its full resolution, and the various global products (median values subtracted). The PDFs are normalised relative to a Gaussian with the same standard deviation, and are offset by ± 1 from their neighbours. Numbers to the right represent the number of available points for comparison in each case.

time, this allows us to see the effect of resolution on the size of the misfit. The results are shown in Figure 7. The long positive tail and high kurtosis do occur when the geoid is poorly resolved, supporting our interpretation. The effect seems to peak at truncations of around degree 300–600, corresponding to length scales of about 40–70 km, but remains even with the full resolution geoid. We interpret this as being a measure of the missing in situ information limiting the resolution of the geoid in some places.

The error standard deviation results show large and continuous improvements with increasing resolution, but begin to plateau at around degree 700, again suggestive of a limit to the added value of the in situ data. The values taken from different parts of the distribution are quite consistent (and lower than the overall standard deviation), apart from the value representative of the upper, more extreme values, confirming that the positive tail has the larger departure from a Gaussian distribution.

In an attempt to determine which are the best models and geoids to use, we rank the 27 possible comparisons of 9 global MDTs with 3 geoids, according to the size of the misfits. The global MDTs include the 7 ocean models described in the Methods section, plus two observational products: AVISO and TUM13.

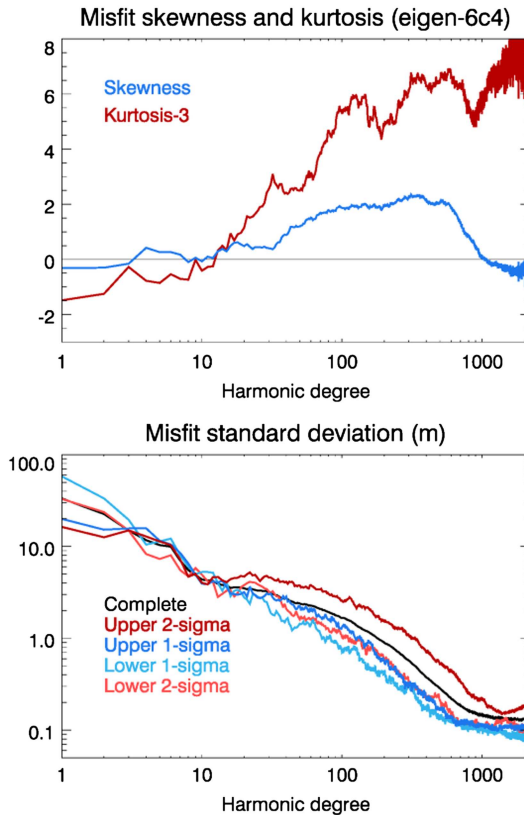


Figure 7. Statistics of misfit between Nemo12a and tide gauge MDTs using the EIGEN-6c4 geoid at different truncations. The standard deviation is shown based on the full PDF, or as the width of the PDF required to contain 34% of data below or above the median, or half the width containing 47.5% below or above the median. These would all be the same for a Gaussian distribution.

The non-Gaussian nature of the PDFs means that no single statistic is representative of the distribution, so we use three different measures: standard deviation, width of the part of the PDF containing the central 68% of the data, and width of the part containing the central 95%. The resultant rankings are shown in Figure 8. The three geoids are EIGEN-6C4 (Foerste 2014), GOCO05c (Fecher, Pail, and Gruber 2017) and EGM2008 (Pavlis et al. 2012). The GOCO05c product was extended from its native resolution of degree 720 using EGM2008 coefficients at higher degrees. All three geoids therefore include information up to degree 2190.

The low-resolution ocean MDT models, LivC, EccoG and LivS, consistently perform poorly, and NemoQ, Aviso and Nemo12a consistently perform well, with TUM13 and Nemo12b in the middle, and Ecco2 closer to the poor end. It is perhaps to be expected that the “observational” products, Aviso and TUM13, should do well, being the most strongly constrained to the real ocean. It is also natural that TUM13 should be slightly

646
647
648
649
650
651
652
653
654
655
656
657
658
659
660
661
662
663
664
665
666
667
668
669
670
671
672
673
674
675
676
677
678
679
680
681
682
683
684
685
686
687
688

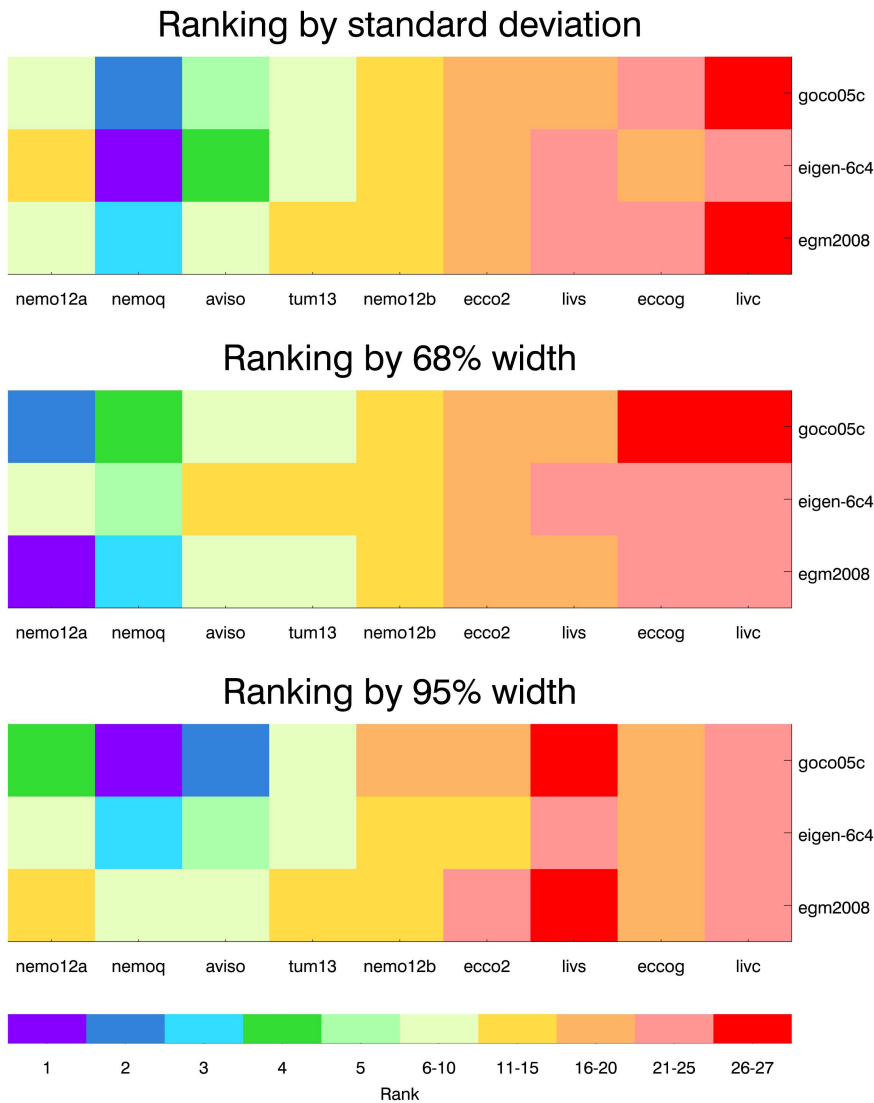


Figure 8. Ranking of quality of comparison of MDTs at tide gauges using three geoids, compared with 9 global products. Three different criteria are used as described in the text.

worse, as it does not include any dynamical constraints, unlike AVISO. However, the ocean model results are interesting. The three low-resolution models perform almost equally poorly, despite assimilation of geodetic data into one of them (EccoG).

The ranking of geoids is less consistent (unsurprisingly given the importance of fine scale information which is derived from very similar, incomplete sources in all cases), with different geoids performing best under different ranking criteria.

Looking back at [Table 1](#), the final column shows the percentage of comparisons which were within 9 cm, after matching the medians. For a

689 Gaussian distribution, this would be 68.2% if 9 cm represented one stand-
690 ard deviation. We can see from this that the best global MDTs have
691 “typical” errors of around 9 cm, if “typical” is defined as analogous to one
692 standard deviation of a Gaussian distribution. This error is similar to the
693 findings for Norway as presented by (Ophaug, Breili, and Gerlach 2015).
694

697 **GOCE++ combined coastal MDT**

698 The satellite derived satellite MDT is generally less accurate in the coastal
699 region due to the sparse coverage of valid altimetry observations. For a
700 description of the satellite MDT see Data and methods section. Because of
701 the degradation in both MSS and geoid artifacts in the coastal region are
702 typically seen as MDT contours crossing the coastline when plotting these.

703 In the GOCE++ project we attempted to derive a coastal MDT by
704 inserting MDT values over land and subsequently smoothing these into the
705 ocean using an iterative spatial filter. The land values can be based on the
706 tide gauge MDT values, the satellite-based MDT in the coastal grid cells, or
707 a combination of both.
708

711 **Land values**

712 In the tide gauge-based solution the tide gauge MDT values are used to fill
713 in the land values. This is done by linearly interpolating the MDT values
714 from either tide gauges or from the MDT model in the coastal zone onto
715 the entire grid of land cells.
716

717 In the satellite-based solution the land value for a given coastal grid
718 point is estimated as the average of the raw MDT grid values in a box cen-
719 tered on the coastal grid cell. The size of this box is by default chosen to
720 be nine times nine grid points which approximately corresponds to a one
721 time one-degree box, as all grids for the test is at 1/8 degree resolution.
722 Hence a local average (defined by the size of the box) for each coastal grid
723 cell is used as a representation of the land value. It is important to notice
724 that the altimetry-based land values will not have the constraining effect
725 provided by the tide gauge MDT values, but only provide an additional
726 smoothing effect ensuring a less noisy MDT along the coast.
727

728 In the combined solution, coastlines without tide gauges are supple-
729 mented with altimetry-based land values as described above. Subsequently
730 the land values along the coast are simply interpolated to all land grid cells
731 using linear or nearest neighbour interpolation.

732 **Filtering**

733 To smooth the raw MDT values a spatial filter is applied. The filter is an
734 average or box filter where the kernel is a nx times ny matrix, where nx
735 and ny are the number of kernel points in the east-west and north-south
736 direction, respectively. In the north-south direction, the size of the filter is
737 fixed with a default value of two while it is scaled by the latitude in the
738 east-west direction. The filter is iteratively applied over both land and
739 ocean grid cells causing the simple average filter to converge toward a
740 Gaussian filter. However, at each iteration, the land values are reset to their
741 original value. This has the effect of maintaining the coastal values and
742 increasing the smoothing in the coastal regions without affecting the open
743 ocean. In general, ten iterations are used.
744

745 **Software**

746 The methodology was implemented in the publically available software
747 “coastMDT” which allows estimation of the coastal MDT in a given region
748 (see the detailed description of the software and how to access it in
749 Appendix 2). [Figure 9](#) shows a flowchart of the software “coastMDT”. The
750 green boxes represent data input to the software; the purple boxes the func-
751 tionality and the blue box the final product. The functionality can briefly
752 be explained in the following steps:
753
754

- 755 • Step 0: The tide gauge data is references to the same ellipsoid as the
756 altimetry data.
- 757 • Step 1: The raw gridded satellite and tide gauge MDTs are derived.
- 758 • Step 2: A region of interest is selected based on a longitude and lati-
759 tude range.
- 760 • Step 3: Land values are estimated based on the methods described in
761 Land values section.
- 762 • Step 4: Filtering over both land and ocean grid cells is applied.
- 763 • Step 5: Plotting, error estimation, and saving of the final MDT.
764

765 **Results**

766 ***The GOCE++ Northeast Atlantic MDT model***

767 As a demonstration of the combined coastal MDT based on the GOCE++
768 approach the raw and filtered solutions are shown for the Northeast
769 Atlantic coastline ([Figure 10](#)). The coastal values in the example are based
770 on a combination of the tide gauge and altimetry as described above. The
771 tide gauges used in this section all lie in the range of numbers 2 to 98 as
772 used in [Figures 3](#) and [4](#) and described in Appendix 1.
773
774

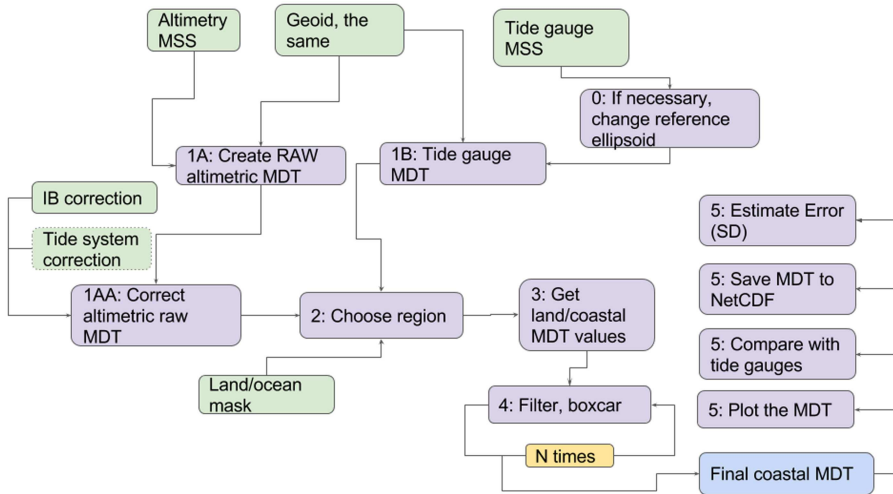


Figure 9. Flowchart of the software “coastMDT”.

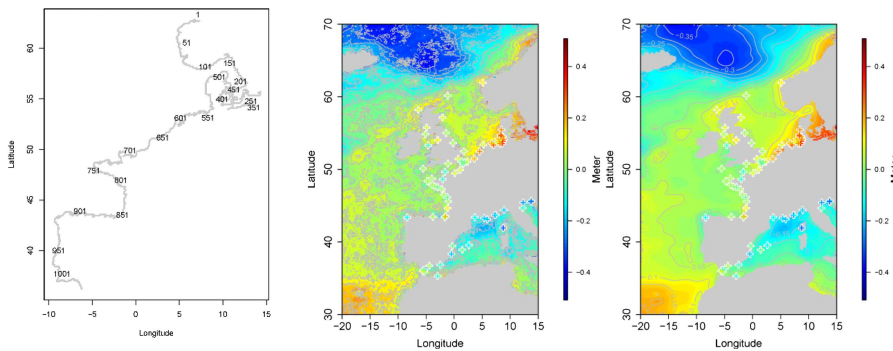


Figure 10. Northeast Atlantic tide gauges and MDT, Left the numbering of the grid points used for the evaluation of the GOCE++ model. Middle. An example of the raw MDT, right, the filtered MDT, where the land values are based on a combination of tide gauges and altimetry. The location of the tide gauges and the corresponding MDT value is shown with crosses.

Figure 11 displays the MDT solutions along the Northeast Atlantic coastline, from Norway to the southern tip of Spain following the labelling in Figure 10. The black curve is the unfiltered MDT corresponding to the raw DTU10MSS-EIGEN4C difference. The blue and red curves represent the coastal MDTs based on a combination of satellite altimetry and tide gauge MDT, and satellite altimetry only, respectively. For comparison, we have included the comparison to a typical satellite MDT. Here we used a MDT derived in the same way as the DTU13MDT (Knudsen et al. 2011) namely based on the satellite MDT values of MSS minus geoid filtered with a Gaussian filter with radius 0.7 degrees and with no land values (shown in green). There is no doubt, that the filtering improves the stability of the MDT solution and that the various filtered solutions generally agree. In

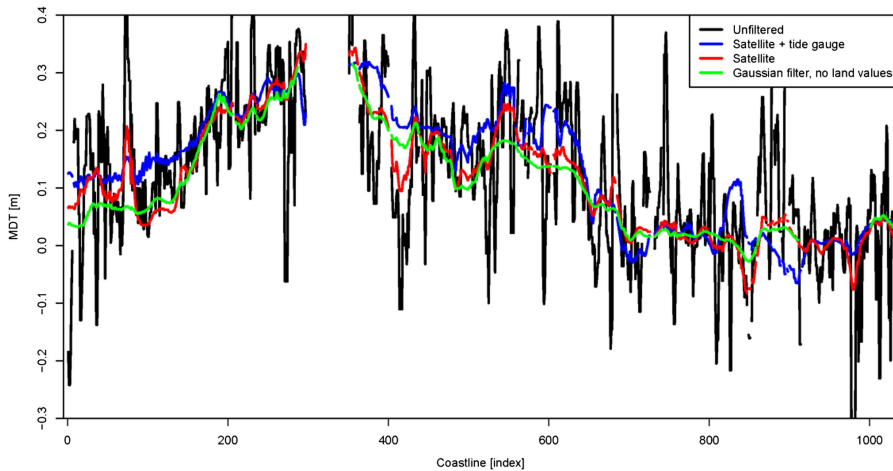


Figure 11. MDT solutions along the Northeast Atlantic. The black curve represents the unfiltered MDT, the blue curve represents the MDT solution where the land values are a combination of the satellite and tide gauge MDT values, the red curve represents the MDT solution where the land values are based on the unfiltered satellite MDT values, and the Green curve represents the MDT solution where a Gaussian filter and no land MDT values has been used.

some places there are deviations up to ~ 10 cm for example index 350–450, 500–650, and 800–900, which corresponds to the coastline along the inner Danish waters, the North Sea, and the Bay of Biscay. However, it is difficult to quantify the quality of the GOCE++ approach visually from this plot.

To evaluate the uncertainty of the MDT solution we apply a bootstrap approach. Since the individual grid points are correlated, we divide the raw MDT data set into blocks, which we assume are uncorrelated. We then create a large number N of artificial data sets by sampling with replacement among the different blocks. For each of the bootstrap data set we derive a filtered MDT solution. In this way, we get a distribution of solutions from which we can estimate the standard deviation of the MDT.

For the validation we select the tide gauges along the Danish, German and French coastlines as the representation of tide gauges is dense here (corresponding to coastal grid points labelled between 300 and 900 in Figure 10). To have independent data for the validation we randomly divide the tide gauges into two groups; 20% for validation and 80% which are used to derive the MDT solution. We can then estimate the RMSE as a measure for the quality of the different solutions. Because the result will depend on which of the tide gauges that are used to derive the solution, we repeat the exercise 100 times. This provides a distribution of the RMSE for the different solutions.

The RMSE distributions for the solutions are shown in Figure 12. In the solutions, land values have been from either altimetry or a combination of altimetry and tide gauges both have medians of 5.8 cm. The MDT without

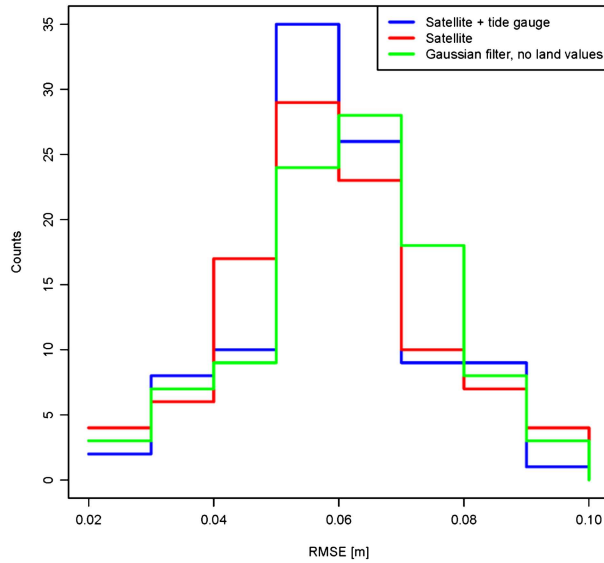


Figure 12. RMSE distributions for the MDT solutions; The MDT using combined tide gauge and satellite altimetry as land values are shown in blue. The MDT using satellite altimetry as land values is shown in red. The Gaussian filtered MDT without land values are shown in green.

land values filtered with a classical Gaussian filter of 0.7 degrees exhibits a median of 6.3 cm. In this investigation we notice a clear improvement if we include land-based MDT values or not. However, we only see a marginal difference if we use satellite altimetry or a combination of satellite altimetry and tide gauge MDT as land values.

Cryosat-2 validation of GOCE++ MDT

Currently SAR altimetry is becoming available with Cryosat-2 and Sentinel-3A/3B to improve the mapping of the short scales in the MSS (Huang 2017). Hence, we evaluate the potential of using SAR altimetry in future geodetic MDT models as SAR altimetry has not been used for MSS computation. In the coastal zone, satellite altimeter data processed with SAR methodology provide water height observations of higher resolution and accuracy compared to the conventional pulse-limited altimeters (Dinardo et al. 2017). Hence, we expect that they should improve the estimation of the MDT in the coastal stripe within 100 km from land. We assess the CryoSat-2 altimetry products over a time interval of 6-years from October 2010 to November 2017 along the North-eastern coasts of the Atlantic Ocean to quantify this.

The SAR data are from ESA Grid Processing on Demand (G-POD) processor enables processed with two different SAR retracking methodologies, called SAMOSA-2 (Ray et al. 2014) and SAMOSA+ (Dinardo et al. 2017).

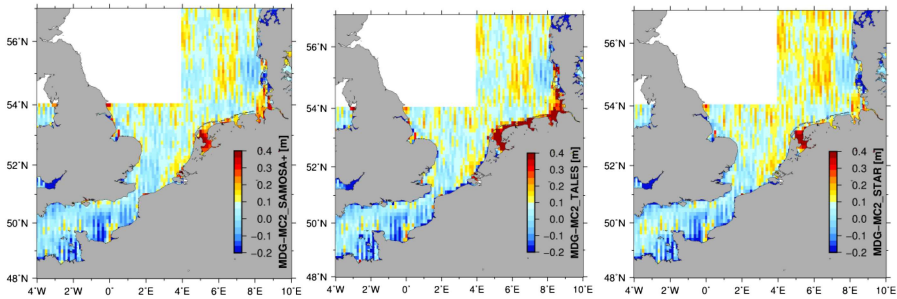


Figure 13. Difference between the GOCE++ MDT and the MDT derived from the three SAR altimetry datasets: SAMOSA+; RDSAR (STAR and TALES) datasets.

The second provides improved coastal data compared to the first, differences are both in the waveforms generation (Hamming weighting window on the burst data prior to the azimuth Fast Fourier Transform (FFT), zero-padding prior to the range FFT, doubling of the extension for the radar range swath) and in the retracking methodology. We use here SAMOSA+ and its corresponding Pseudo-LRM data, also called reduced SAR altimetry (RDSAR). This latter is generated by the TUDABo processor (<http://wiki.services.eoportal.org/tiki-index.php?page=G-POD+services>) and retracked using the TU-Darmstadt Adaptive Leading Edge Sub-waveform retracker (TALES) and Spatio-Temporal Altimeter Waveform Retracking (STAR) sub-waveform retracker (Fenoglio-Marc and Buchhaupt 2017; cher, Uebbing, and Kusche 2017). The quality of RDSAR and LRM data are comparable. LRM was disregarded near coast in the estimation of past MSS. The impact of the new SAMOSA+ data quality on the MDT estimation is seen from an estimate of a new MDT by averaging the 6 years of CryoSat-2 data on a 0.25×0.25 degree grid. We then compare it to the reference geodetic MDT output of this project. The standard deviation of differences between the reference MDT surface and the MDT surfaces constructed from SAMOSA+, TALES and STAR open sea and coastal data are 6.7 cm for SAMOSA+, 8.5 cm for TALES and 6.9 cm for STAR, respectively. The largest difference between the reference MDT and the new MDT surfaces is in the coastal zone. Figure 13 shows the difference between the reference MDT and the new MDT surfaces. The best agreement with the reference MDT (smallest differences in the German Bight) is obtained using the SAMOSA+ data (Figure 13, left) followed by the RDSAR STAR data, while with RDSAR TALES the agreement is lower.

Discussion, recommendations, and conclusion

In the GOCE++ project we have tested a new approach to improve the MDT in the coastal zone, where the solution is based on both satellite altimetry and tide gauge data. The tide gauge MDT values are integrated

947 into the geodetic MDT by inserting these as land values and subsequently
948 using an iterative average filter to smooth the tide gauge MDT values into
949 the altimetry-based MDT. The approach was evaluated for the Northeast
950 Atlantic coast where a dense representation of tide gauges is present. A val-
951 idation of the coastal MDT was conducted by comparing the solution to
952 that obtained from tide gauges. To ensure independent data for the valid-
953 ation only 80% of the tide gauges were included in the MDT solution. The
954 new approach showed a small but clear improvement in terms of RMSE
955 compared to the classical spatial Gaussian filter.

956 In this investigation, the land values were assigned using linear interpol-
957 ation, which is not optimal when the tide gauges are unevenly distributed
958 along the coastline or if the distance between them is large (see the hetero-
959 geneous distribution of the tide gauges on [Figure 2](#)). An improved future
960 approach could be to consider the correlation pattern potentially from
961 ocean model MDTs when interpolating the land values. The GOCE++
962 approach to derive a coastal MDT based on altimetry and tide gauge data
963 was implemented as an R package “coastMDT” which is freely available for
964 further research. The package can be used with the provided test data used
965 here or with data provided by the user.

966 The typical misfit between tide gauge and satellite or oceanographic
967 MDT was found to be around 9 cm. This misfit was found to be mainly
968 due to small scale geoid errors. Similarly, a single tide gauge places only
969 weak constraints on the coastal dynamic topography, especially when the
970 non-Gaussian nature of the errors means that much larger misfits are pos-
971 sible. Optimal use of the tide gauges thus relies on exploiting the coherence
972 of the MDT along the coast, together with a good quantification of errors
973 in the tide gauge values. Preliminary analyses have shown that sea level
974 variations at tide gauges bear very different relationships to nearby open
975 ocean values from satellite altimetry, depending on the site considered.

976 Where variability at gauges agrees with open ocean altimetry, it seems
977 safe to assume that the tide gauge mean should also reflect the ocean mean
978 dynamic topography. Where it does not, there are three possibilities: the
979 data quality may be poor, the local geoid error may be large, or local
980 coastal processes may be important. Possible processes are wave setup and
981 low salinity intrusions due to freshwater input from rivers, both of which
982 have been suggested to contribute tens of centimetres in places. In fact,
983 some gauges are far enough up rivers that they may reflect river flow more
984 directly. Altimetry closer to the coast would help to distinguish between
985 these possibilities.

986 Improved mapping of coastal currents and short scale geoid signals will
987 be important to improve coastal MDT. This can be done through the inte-
988 gration with very high-resolution ocean model. Local analysis into the
989

990 Norwegian MDT demonstrated the value of SAR altimetry in mapping
991 local coastal topographies from CryoSat-2 (Idžanović, Ophaug, and
992 Andersen 2017). Along the Norwegian coast strong levelling ties between
993 tide gauges permit a comparison, which is not dependent on direct GPS
994 measurements at each gauge. The addition of measurements very close to
995 the coast was found to help in avoiding errors due to coastal currents, seen
996 in both the satellite data and ocean model. The remaining error, however,
997 was found to be dominated by small-scale geoid error, which can only be
998 addressed by local gravity measurements.

999 Similar investigations into Australian coastal MDT also highlighted the
1000 small-scale geoid error, at larger amplitude in this case, with sporadic mis-
1001 matches of 0.1–0.2 m (Filmer et al. 2018). In some cases, these were found
1002 to be in regions of complex coastal geometry (in one case the gauge is
1003 some distance from the coast). In this investigation, we found that addition
1004 of CryoSat-2 data had the potential to improve the coastal resolution. In
1005 this case, however, another issue was also identified: the availability of tide
1006 model data was found to be a limiting factor, which was overcome by
1007 switching from the GOT4.8 to the FES2012 tidal model. This highlights the
1008 importance of reassessing altimeter correction models as new, more-coastal
1009 data become available.

1010 The biggest challenge for unified calculation of a coastal and global
1011 MDT is clearly the lack of small-scale geoid information for comparison
1012 with point measurements from tide gauges. This is a problem with varying
1013 geographical impact, which will ultimately only be overcome by use of local
1014 measurements; either of gravity in a region surrounding the point in ques-
1015 tion, or of geopotential at the point (see later).

1016 A second challenge is the limited number of tide gauges with GPS ties
1017 (Woodworth et al. 2017). We have identified 302 such gauges in this pro-
1018 ject, in comparison to 1007 datum-controlled records, which overlap the
1019 satellite altimetry era (1993 onwards). The vertical velocity of the GNSS sta-
1020 tion used was known for only 141 of these 302 tide gauges (47%), the
1021 epoch of the height for only 160 (53%). Thus, for a significant number of
1022 the selected tide gauges, it was not possible to propagate the height at the
1023 chosen epoch 2005.5. Actually, 90% of the 400 coastal (closer than 20 km)
1024 ULR6 vertical velocities being in absolute value below 3.5 mm year^{-1} , it
1025 can be assumed that the maximum error of an ellipsoidal height at an
1026 unknown epoch with an unknown velocity is around 4 cm if we consider
1027 that this unknown epoch is between 1995.0 and 2017.0 (and so distant to a
1028 maximum period of 11.5 years from the chosen period 2005.5). Even with-
1029 out additional data, the present investigations have highlighted a number
1030 of ways in which immediate progress can be made based on observations,
1031 which are currently available or will become available in the next few years.
1032

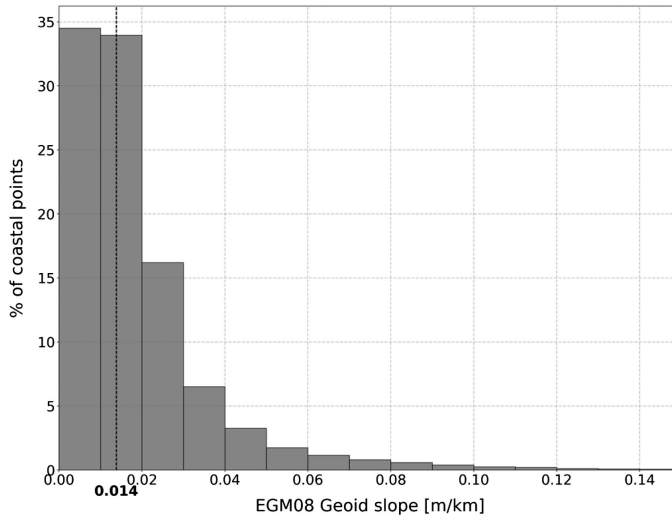


Figure 14. Histogram of the geoid slopes in coastal areas.

The accuracy of the tide gauge location can also have an impact on the MDT value through the geoid value extraction. The locations used in this study were taken from the PSMSL and SONEL databanks which strives to locate the tide gauges as accurate as possible. To estimate the impact of possible remaining errors in the locations of the tide gauges used, a geoid slope map has been computed over a global 40 km wide coastal strip from the EGM2008 model (Pavlis et al. 2012). The histogram on Figure 14 shows a median equal to 0.014 m km^{-1} .

A number of recommendations for future directions on both short-term horizon of a few years, and a longer-term decadal time scale can be found from the GOCE++ results at (<http://gocehsu.eu>). The recommendations detail our view on how to use and our strategies to improved GNSS coverage at tide including strategies to account for local vertical land movement when computing tide-gauge MDT.

The strategies for deriving an optimal MDT will play out very differently in different regions. In well-surveyed regions with many tide gauges, the tide gauge data is likely to play a significant role in constraining the coastal solutions. In poorly surveyed regions, where tide gauge data are sparse, there will be no along-coast averaging effect, and the sporadic measurements with correspondingly large errors (given the lack of information about short length-scale variability) are unlikely to make a significant contribution. As an example, the Pacific island measurements appear to have both random and systematic errors of order 0.1 m. On the other hand, model data show that the MDT remains within 0.02 m of the coastal MDT out to distances of hundreds of kilometres from most islands meaning that the satellite data will produce the greater constraint. In order for isolated

1076 tide gauges to make a significant contribution, it is crucial that local geoid
 1077 information be improved, and the improvement be quantified.

1078 **Acknowledgements**

1081 The authors are thankful to Phil Woodworth for valuable suggestions. The authors acknow-
 1082 ledge the support to the ESA STSE GOCE ++ DYCOT project via ESA contract No
 1083 4000114331//15/NL/FF/gp. They also acknowledge the SONEL (<http://www.sonel.org>) and
 1084 RENAG (<http://webrenag.unice.fr>) services for providing GPS data and geodetic ties at tide
 1085 gauges. Hongyang Lin, Mick Filmer, Marc Véronneau are warmly thanked for providing
 1086 geodetic ties respectively in Japan and USA, Australia and Canada.

1087 **Disclosure statement**

1089 No potential conflict of interest was reported by the authors.

1091 **References**

- 1092 Altamimi, Z., X. Collilieux, and L. Métivier. 2011. ITRF2008: An improved solution of the
 1093 international terrestrial reference frame. *Journal of Geodesy* 85 (8):457–473.
- 1094 Amjadiparvar, B., E. V. Rangelova, M. G. Sideris, and M. Véronneau. 2013. North
 1095 American height datums and their offsets: The effect of GOCE omission errors and sys-
 1096 tematic levelling effects. *Journal of Applied Geodesy* 7 (1):39–50. doi:10.1515/jag-2012-
 1097 0034
- 1098 Andersen, O. B., and P. Knudsen. 2009. The DNSC08 mean sea surface and mean dynamic
 1099 topography. *Journal of Geophysical Research* 114:C11. doi:10.1029/2008JC005179
- 1100 Andersen, O. B., P. Knudsen, and L. Stenseng. 2016. *The DTU13 MSS (mean sea surface)*
 1101 *and MDT (mean dynamic topography) from 20 years of satellite altimetry*. IAG Symposia,
 1102 1–10. Springer Verlag.
- Q5 1103 Bingham, R. J., and K. . 2006. Mean dynamic topography: Intercomparisons and
 1104 errors. *Philosophical Transactions of the Royal Society A* 364 (1841):903–916. doi:10.1098/
 1105 rsta.2006.1745.
- 1106 Bingham, R. J., P. Knudsen, O. B. Andersen, and R. Pail. 2011. An initial estimate of the
 1107 North atlantic steady-state geostrophic circulation from GOCE. *Geophysical Research*
 1108 *Letters* 38 (1):L01606. doi:10.1029/2010GL045633.
- 1109 Dinardo, S., L. Fenoglio-Marc, C. Buchhaupt, M. Becker, R. Scharroo, J. Fernandez, and J.
 1110 Benveniste. 2017. Coastal SAR and PLRM altimetry in German bight and Western Baltic
 1111 sea, advance in space research. *Special Issue CryoSat-2* doi:10.1016/j.asr.2017.12.018.
- Q6 1112 Ekman, . 1989. Impacts of geodynamic phenomena on systems for height and gravity.
 1113 *Bulletin Géodésique* 63 (3):281–296. doi:10.1007/BF02520477.
- 1114 Featherstone, W. E., and M. S. Filmer. 2012. The North-South tilt in the Australian height
 1115 datum is explained by the ocean's mean dynamic topography. *Journal of Geophysical*
 1116 *Research* 117: C08035. doi:10.1029/2012JC007974.
- 1117 Fecher, T., R. Pail, and T. Gruber. 2015. Global gravity field modeling based on GOCE and
 1118 complementary gravity data. *International Journal of Applied Earth Observation and*
Geoinformation 35 (A):120–127. doi:10.1016/j.jag.2013.10.005.

- 1119 Fecher, T., R. Pail, and T. Gruber. 2017. GOCO05c: A new combined gravity field model
 1120 based on full normal equations and regionally varying weighting. *Surveys in Geophysics*
 1121 38 (3):571. doi:10.1007/s10712-016-9406-y
- 1122 Fenoglio-Marc, L., and C. Buchhaupt. 2017. TUDaBo SAR-RDSAR for G-POD, altimetry
 1123 coastal and open ocean performance. *Algorithm Theoretical Basis Document (ATBD)*
 1124 Q7 SAR-RDSAR for GPOD, EOEP-SEOM-EOPS-TN-17-046, Issue: 1.3
- 1125  er, M. E., C. W. Hughes, P. L. Woodworth, W. E. Featherstone, and R. J. Bingham.
 1126 Q8 2018. Comparison of oceanographically and geodetically derived ocean mean dynamic
 1127 topography at australian tide gauges. *Journal of Geodesy* doi:10.1007/s00190-018-1131-5. 
- 1128 Foerste, C. 2014. EIGEN-6C4: The latest combined global gravity field model including
 1129 GOCE data up to degree and order 1949 of GFZ Potsdam and GRGS Toulouse. *EGU*
 1130 Q9 *General Assembly Conference Abstracts* 16.
- 1131  ach, C., and R. Rummel. 2013. Global height system unification with GOCE: A simula-
 1132 tion study on the indirect bias term in the GBVP approach. *Journal of Geodesy* 87 (1):
 1133 57–67. doi:10.1007/s00190-012-0579-y
- 1134 Gruber, T., C. Gerlach, and R. H. N. Haagmans. 2012. Intercontinental height datum con-
 1135 nection with GOCE and GPS-levelling data. *Journal of Geodetic Science* 2 (4):270–280.
 1136 doi:10.2478/v10156-012-0001-y
- 1137 Holgate, S. J., A. Matthews, P. L. Woodworth, L. J. Rickards, M. E. Tamisiea, E. Bradshaw,
 1138 P. R. Foden, K. M. Gordon, S. Jevrejeva, and J. Pugh. 2013. New data systems and prod-
 1139 ucts at the permanent service for mean sea level. *Journal of Coastal Research* 288:
 1140 493–504.
- 1141 Huang, J. 2017. Determining coastal mean dynamic topography by geodetic methods.
 1142 *Geophysical Research Letters* 44 (21):11,125–128. doi:10.1002/2017GL076020
- 1143 Idžanović, M., V. Ophaug, and O. B. Andersen. 2017. The coastal mean dynamic topog-
 1144 raphy in Norway observed by CryoSat-2 and GOCE. *Geophysical Research Letters* 44
 1145 (11):5609–5617. doi:10.1002/2017GL073777
- 1146 IERS 2010. IERS Conventions (2010). In *International earth rotation service technical note*,
 1147 Q10 ed. G. Petit and B. Luzum, vol. 36, 179. 
- 1148 Knudsen, P., R. Bingham, O. B. Andersen,  M.-H. Rio. 2011. A global mean dynamic
 1149 topography and ocean circulation estimation using a preliminary GOCE gravity model.
 1150 *Journal of Geodesy* 85 (11): 861–879. doi:10.1007/s00190-011-0485-8
- 1151 Köhl, A., D. Stammer, and B. Cornuelle. 2007. Interannual to decadal changes in the
 1152 ECCO global synthesis. *Journal of Physical Oceanography* 37 (2):313–337. doi:10.1175/
 1153 JPO3014.1
- 1154 Lin, H., K. R. Thompson, J. Huang, and M. Véronneau. 2015. Tilt of mean sea level along
 1155 the pacific coasts of North America and Japan. *Journal of Geophysical Research: Oceans*
 1156 120 (10):6815–6828. doi:10.1002/2015JC010920.
- 1157 Madec, G. 2008. *NEMO ocean engine, note du pole de modelisation*. Vol.27, 1288–1619.
 1158 Paris, France: Inst. Pierre-Simon Laplace.
- 1159 Marshall, J., A. Adcroft, C. Hill, L. Perelman, and C. Heisey. 1997a. A finite-volume,
 1160 incompressible navier stokes model for studies of the ocean on parallel computers.
 1161 *Journal of Geophysical Research: Oceans* 102 (C3):5753–5766. doi:10.1029/96JC02775.
- Marshall, J., C. Hill, L. Perelman, and A. Adcroft. 1997b. Hydrostatic, quasi-hydrostatic,
 and nonhydrostatic ocean modelling. *Journal of Geophysical Research: Oceans* 102 (C3):
 5733–5752. doi:10.1029/96JC02776.
- Menemenlis, D., I. Fukumori, and T. Lee. 2005a. Using green's functions to calibrate an
 ocean general circulation model. *Monthly Weather Review* 133 (5):1224–1240. doi:
 10.1175/MWR2912.1.

- 1162 Menemenlis, D., C. Hill, A. Adcroft, J.-M. Campin, B. Cheng, B. Ciotti, I. Fukumori, P.
1163 Heimbach, C. Henze, A. Köhl, et al. 2005b. NASA supercomputer improves prospects
1164 for ocean climate research. *Eos, Transactions American Geophysical Union* 86 (9):89–96.
1165 doi:10.1029/2005EO090002.
- 1166 Ophaug, V., K. Breili, and C. Gerlach. 2015. A comparative assessment of coastal mean
1167 dynamic topography in Norway by geodetic and ocean approaches. *Journal of*
1168 *Geophysical Research: Oceans* 120:12.
- 1169 Pavlis, N. K., S. A. Holmes, S. C. Kenyon, and J. K. Factor. 2012. The development and
1170 evaluation of the earth gravitational model 2008 (EGM2008). *Journal of Geophysical*
1171 *Research* 117:B04406. doi:10.1029/2011JB008916.
- 1172 Ray, C., C. Martin-Puig, M. P. Clarizia, G. Ruffini, S. Dinardo, C. Gommenginger, and J.
1173 Benveniste. 2014. SAR altimeter backscattered waveform model. *IEEE Transactions on*
1174 *Geoscience and Remote Sensing* 53 (2):911–919.
- 1175 Roscher, R., B. Uebbing, and J. Kusche. 2017. STAR: Spatio-temporal altimeter waveform
1176 retracking using sparse representation and conditional random fields. *Remote Sensing of*
1177 *Environment* 201:148–164. doi:10.1016/j.rse.2017.07.024.
- 1178 Rummel, R. 2012. Height unification using GOCE. *Journal of Geodetic Science* 2 (4):
1179 355–362. doi:10.2478/v10156-011-0047-2
- 1180 Sanchez-Reales, J. M., O. B. Andersen, and M. I. Vigo. 2016. Improving surface geostrophic
1181 current from a GOCE-Derived mean dynamic topography using Edge-Enhancing diffu-
1182 sion filtering. *Pure and Applied Geophysics* 173 (3):871–884. doi:10.1007/s00024-015-
1183 1050-9.
- 1184 Santamaría-Gómez, A., M. Gravelle, S. Dangendorf, M. Marcos, G. Spada, and G.
1185 Wöppelmann. 2017. Uncertainty of the 20th century sea-level rise due to vertical land
1186 motion errors. *Earth and Planetary Science Letters* 473:24–32.
- 1187 Smith, D. M., and J. M. Murphy. 2007. An objective ocean temperature and salinity ana-
1188 lysis using covariances from a global climate model. *Journal of Geophysical Research* 112:
1189 C02022. doi:10.1029/2005JC003172.
- 1190 Woodworth, P. L., M. Gravelle, M. Marcos, G. Wöppelmann, and C. W. Hughes. 2015.
1191 The status of measurement of the Mediterranean mean dynamic topography by geodetic
1192 techniques. *Journal Geodesy* 89 :1–17. doi:10.1007/s00190-015-0817-1.
- 1193 Woodworth, P. L., C. W. Hughes, R. J. Bingham, and T. Gruber. 2013. Towards worldwide
1194 height system unification using ocean information. *Journal of Geodetic Science* 2 (4):
1195 302–318.
- 1196 Woodworth, P. L., G. Wöppelmann, M. Marcos, M. Gravelle, and R. M. Bingley. 2017.
1197 Why we must tie satellite positioning to tide gauge data. *Eos* 98. doi:10.1029/
1198 2017EO064037
- 1199 Q11  Wöppelmann, G., and M. Marcos. 2016. Vertical land motion as a key to understanding
1200 sea level change and variability. *Reviews of Geophysics* 54 (1):64–92. doi:10.1002/
1201 2015RG000502.
- 1202 Wunsch, C., and D. Stammer. 1997. Atmospheric loading and the oceanic “inverted
1203 barometer” effect. *Reviews of Geophysics* 35 (1):79–107. doi:10.1029/96RG030337.
1204

Appendix 1

Tide gauge locations.

The locations of the 302 tide gauges used in this study, showing the numbering scheme used in the various plots within the article. The solid circles represent the first tide gauge in each colour.

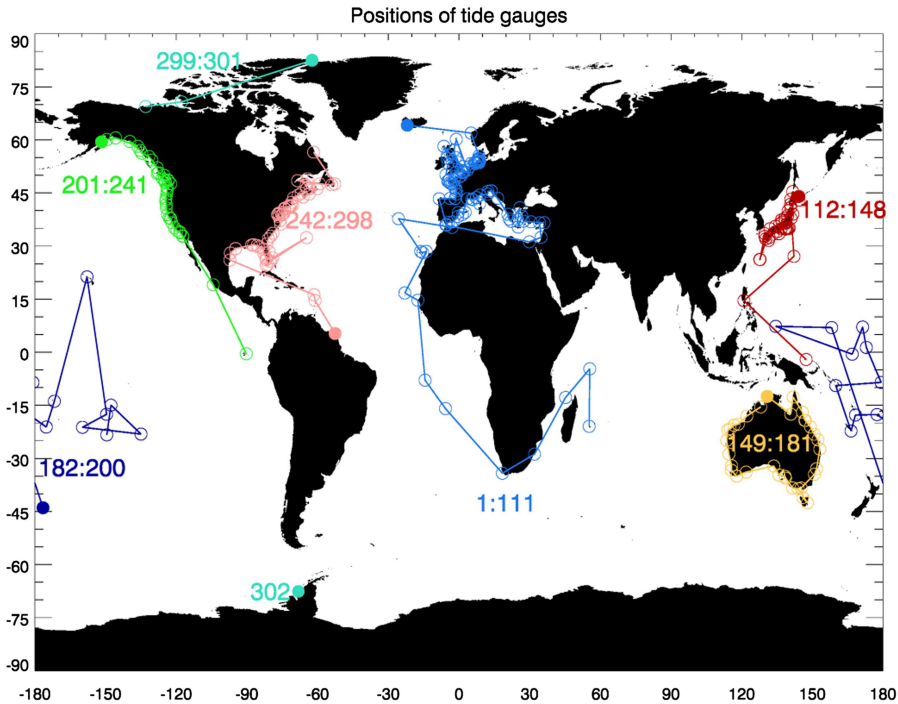


Figure A1. Positions of tide gauges used in this study, showing the numbering scheme used in plots. The solid circles represent the first tide gauge in each colour.

Appendix 2

Software

The methodology described in the previous sections was implemented in a software package “coastMDT” written in the open source language “R”. The software is freely available from GitHub (<https://github.com/cavios/coastMDT>) including installation instructions and documentation.

The package “coastMDT” offers the user the possibility to derive a geodetic MDT for a selected region of interest. In relation to the package a collection of data sets is also available including the MSS/MDT values at the tide gauge stations for the combined GOCO05C (Fecher et al.2017) and EIGEN 6C4 geoids (Foerste 2014) as well as the DTU 10 & 15MSS (Andersen et al.2016). The gridded datasets are all given with a resolution of a $1/8 \times 1/8$ degree. A detailed description of the functions in the package is found in the CoastMDT user manual and complete example of how to use the package to derive the MDT is described in the coastMDT tutorial.